Sizing Energy Storage to Mitigate Wind Power Forecast Error Impacts by Signal Processing Techniques

Hamideh Bitaraf, *Student Member, IEEE*, Saifur Rahman, *Fellow, IEEE*, and Manisa Pipattanasomporn, *Senior Member, IEEE*

***Abstract*—This paper proposes to use discrete Fourier transform (DFT) and discrete wavelet transform (DWT) methods to schedule grid-scale energy storage systems to mitigate wind power forecast error impacts while considering energy storage properties. This is accomplished by decomposing the wind forecast error signal to different time-varying periodic components to schedule sodium sulfur (NaS) batteries, compressed air energy storage (CAES), and conventional generators. The advantage of signal processing techniques is that the resultant decomposed components are appropriate for cycling of each energy storage technology. It is also beneficial for conventional generators, which are more efficient to operate close to rated capacity. The tradeoff between installing more energy storage units and decreasing the wind spillage, back-up energy, and the standard deviation of residual forecast error signal is analyzed. The NaS battery life cycle analysis and CAES contribution on increasing NaS battery lifetime are studied. The impact of considering the frequency bias constant to allow small frequency deviations is also investigated. To showcase the applicability of the proposed approach, a simulation case study based on a real-world 5-min interval wind data from Bonneville Power Administration (BPA) in 2013 is presented.**

***Index Terms*—Back-up energy, discrete Fourier transform (DFT), discrete wavelet transform (DWT), frequency bias constant, grid-scale energy storage, life cycle analysis, wind power forecast error, wind spillage.**

I. Introduction

HIGH WIND penetration is a potential future scenario that can result from various energy and environmental policies. Denmark, Portugal, and Spain are the top three countries with the highest percentage of electricity production from wind farms [1]. In Denmark, wind power provided 33.2% of its annual electricity consumption in 2013 and is expected to reach 50% by 2020 and 100% by 2035 [1], [2]. U.S. annual wind generation in 2012 was 3.5% [1]. "In Texas, wind power is approaching 10% of the state's total electricity generation. Iowa is producing 25% of its power from wind, and overall, nine states obtain 10% or more of their electricity from wind energy" [1].

Manuscript received February 21, 2015; revised May 11, 2015; accepted June 20, 2015. Date of publication July 14, 2015; date of current version September 16, 2015. This work was supported in part by the U.S. National Science Foundation under Grant OISE-1104023. Paper no. TSTE-00129-2015.

The authors are with the Bradley Department of Electrical and Computer Engineering, Virginia Tech, Blacksburg, VA 24060 USA, and also with the Advanced Research Institute, Virginia Tech, Arlington, VA 22203 USA (e-mail: bhamideh@vt.edu; srahman@vt.edu; mpipatta@vt.edu).

Color versions of one or more of the figures in this paper are available online at http://ieeexplore.ieee.org.

Digital Object Identifier 10.1109/TSTE.2015.2449076

High level of uncertainty in wind power output results in wind power forecast errors. Solutions to overcome this uncertainty may include improvement in wind forecasting, use of subhourly scheduling, increase in system reserve, deployment of energy storage technologies, or some combinations thereof. Energy storage can absorb excess wind power when the actual wind power output is more than the forecasted one. It can also inject required power when the actual wind power output is less. Proper sizing of energy storage can help reduce the spillage of excess wind energy and avoid paying a penalty when there is wind energy deficiency.

In the literature, sizing of energy storage units is solved by optimization approaches considering investment, operation, and penalty costs [3]–[8] to maximize the revenue or smooth the output power. Energy storage sizing to allow the combined wind and storage output meet the predicted hour-ahead or day-ahead power output has been addressed in [9]–[12]. Variety of heuristic optimization methods [13], [14] and game theory approaches [15], [16] have been used to solve the energy storage sizing problem in a system with high wind penetration. Sizing energy storage based on pre- and postcompensation to minimize hourly wind forecast error energy is studied in [17]. Sizing Li-ion batteries based on statistical analysis of wind power forecast error is studied in [18].

Hybrid energy storage sizing can be solved by signal processing approaches, which are based on the concept that the efficient operation of energy storage or conventional units depends on their cycling. This is the advantage of signal processing techniques that extract control signals with appropriate cycling for a specific type of energy storage technology. The discrete Fourier transform (DFT) to mitigate wind power forecast error is proposed in [19]. Planning of energy storage and diesel generator capacities based on DFT to supply a load in a microgrid with wind integration has been addressed in [20]. Discrete wavelet transform (DWT) was used for data filtering of day-ahead electricity price forecasting in [21]. DWT has also been used to control storage for smoothing the fluctuation of wind farm output [23]. Comparing signal processing techniques has been studied for islanding detection in [23], but not for energy storage sizing.

The energy storage sizing to mitigate wind forecast error using DFT and DWT methods is discussed in this paper. The wind power forecast error signal is decomposed into intra-hour, intra-day, and slow-cycling components. The intra-hour and intra-day components are time-varying periodic components

with zero total energy, which are suitable to control sodium sulfur (NaS) battery and compressed air energy storage (CAES), respectively. NaS is a chemical energy storage with no barrier to switch between charge and discharge modes, with high ramp rate. Hence, it is a good candidate for intra-hour component. However, the limited life cycle of NaS battery will limit how frequently this battery can be charged or discharged. On the other hand, CAES is a mechanical energy storage device that has larger rated energy capacity compared to NaS. This is a good candidate for intra-day component. The idle time to switch between charge and discharge modes is 20 min, which limits its flexibility of operation. The slow-cycling component is supposed to be supplied by conventional generators, which are more efficient while operating at high mean generation level.

The contributions and advantages of the proposed method in this paper compared with other existing signal processing techniques in [19], [20], and [22] are summarized as follows.

1) Considering the detailed properties of each energy storage technology: These properties include ramp rate, idle time for CAES to switch between charge and discharge modes, and maximum and minimum state of charge (SoC), in addtion to efficiency and rated power and energy capacity.
2) Choosing a specific wavelet function for DWT: The wavelet function in [22] is chosen based on correlation with the net load signal. Haar wavelet function is selected in this paper because this step-shape wavelet function results in intra-day components that are constant for a specific duration. This characteristic is convenient to schedule mechanical energy storage units as CAES. DFT and DWT with other non-Haar wavelet functions change the control command at every time interval, which is too frequent for the CAES unit to operate.
3) Analyzing the impacts of energy storage by different scenarios: The results presented in [19], [20], and [22] are required rated power and energy capacity that fully compensate the decomposed components, even the infrequent ones. This paper analyzes the impacts of different combinations of energy storage units on reducing wind spill, back up energy, and standard deviation of the residual forecast error signal. Back-up energy is total additional energy provided by thermal or hydro generators to make up for the generation shortage.
4) Calculating the service life of NaS: The battery service life is very important in long-term planning. The impact of increasing the number of energy NaS and CAES units on NaS life cycle is investigated in this paper.
5) Considering frequency bias constant: This factor can alleviate the wind power forecast error impacts. It allows small frequency deviation (0.1 Hz) from 60 Hz to reduce wind spill and back-up energy.

This paper is organized as follows. Sections II and III describe the methodology and the storage sizing algorithm, respectively. The case study and discussion are presented in Section V.

II. DFT and DWT Analysis

A. DFT Analysis

DFT analysis changes time domain to frequency domain with sinusoidal basic function. First, DFT of the signal is derived as shown in (1), and then it is passed through high-pass, band-pass, and low-pass filters to get different components. Finally, the resultant components are converted into the time domain using inverse DFT as follows:

$$X_k = \sum_{n=0}^{N-1} x_n \,.\, e^{-i2\pi kn/N},\ k \in Z \tag{1}$$

$$x_n = \frac{1}{N} \sum_{n=0}^{N-1} X_k \,.\, e^{i2\pi kn/N}, \quad n \in Z. \tag{2}$$

B. DWT Analysis

DWT changes the signal domain to time-frequency plane by scaling and shifting the basic wavelet function. The set of basic wavelet function is defined as [24]

$$\Psi_{j,k,t} = \frac{1}{\sqrt{2^j}} \Psi \left(\frac{t - k2^j}{2^j} \right) \tag{3}$$

where Ψ is the wavelet function, 2^j is the scaling factor of t, and $k2^j$ is the translation in t. The factor $2^{j/2}$ maintains the norm of the wavelet at different scales. The Haar wavelet function is described in the following [24]:

$$\Psi_{\text{Haar},t} = \begin{cases} 1, & \text{if } 0 < t < 0.5 \\ -1, & \text{if } 0.5 < t < 1 \\ 0, & \text{otherwise.} \end{cases} \tag{4}$$

In this paper, the DWT decomposition with Haar wavelet function is used among other wavelet functions. Hence, the decomposed signals are shifted and scaled version of Haar wavelet function which is step-shape and constant for each half period as (4). This characteristic may be desirable to control large-scale mechanical energy storage unit with barriers to switch between operation modes frequently. A signal can have the representation seen in the following [24]:

$$f_t = \sum_{j,k} a_{j,k} \Psi_{j,k,t} \tag{5}$$

where the two-dimensional (2-D) coefficient $a_{j,k}$ is called DWT of f_t. It is calculated by inner products as follows [24]:

$$a_{j,k} = \langle \Psi_{j,k,t}, f_t \rangle \,. \tag{6}$$

The signal is decomposed into approximate and detailed signals as follows [24]:

$$f_t = A_{n,t} + \sum_{j=1}^{n} D_{j,t} \tag{7}$$

where

$A_{n,t}$ approximate signal at nth level decomposition at time t;
$D_{j,t}$ detailed signal at jth level decomposition ($j = 1, \ldots, n$) at time t;
n level of DWT decomposition.

III. Energy Storage Sizing Algorithm

The difference between wind power and its hour-ahead fore cast represents the wind power forecast error as follows:

$$p_{\mathrm{wfe},t} = p_{\mathrm{aw},t} - p_{\mathrm{fw},t} \quad \forall t \tag{8}$$

where

$p_{\mathrm{wfe},t}$ wind power forecast error signal at time t;
$p_{\mathrm{aw},t}$ actual wind power signal at time t;
$p_{\mathrm{fw},t}$ forecasted wind power signal at time t.

The wind power forecast error is formulated in an area control error (ACE) as expressed in (9) [19]. The balancing authority is expected to return ACE to zero by utilizing contingency reserve to compensate for the error

$$-\mathrm{ACE} = -(I_a - I_s) + 10\beta(f_a - f_s) \tag{9}$$

where

I_a actual interchange in MW;
I_s scheduled interchange in MW;
f_a actual system frequency in Hz;
f_s scheduled system frequency in Hz;
β system frequency bias constant in MW/0.1 Hz.

The frequency bias constant allows the incorporation of intermittent renewable energy sources into a power system with a small frequency deviation of up to 0.1 Hz. Many balancing authorities take a simple approach and calculate this as 1% of the forecasted peak load of the year [24]. Consequently, a 100-MW [1% of Bonneville Power Administration (BPA) 2013 peak load] power mismatch in the system can be allowed according to frequency bias constant.

The detailed energy storage sizing algorithms for DWT and DFT methods are defined as follows.

A. Energy Storage Sizing Algorithm Based on DWT

Step 1) Find $p_{\mathrm{wfe},t}$ as described in (8).
Step 2) Decompose $p_{\mathrm{wfe},t}$ using Haar as a wavelet function to approximate and detailed signals as shown in (7). The period of jth detailed signal is 2^j times the data time resolution. The duration of its constant command is 2^{j-1} times the data time resolution. The approximate signal with n-level of decomposition is constant for 2^n times the data time resolution. Hence, the level of DWT decomposition is chosen to be 8, which results in an approximate signal changing every 21 h and 20 min. This decomposition level keeps the period of detailed signals less than a day. As a result, intra-hour and intra-day components are extracted from the detailed signals with 8-level of decomposition.

TABLE I
DFT Methodology Filters

Filter	f_l (MHz)	f_u (MHz)	$1/f_l$ (h:min)	$1/f_u$ (h:min)
High pass	0.208	–	$2^4 \times 5$ min = 01:20	–
Band pass	0.208	0.013	$2^4 \times 5$ min = 01:20	$2^8 \times 5$ min = 21:20
Low pass	–	0.013	–	$2^8 \times 5$ min = 21:20

Step 3) Derive high-, medium-, and low-frequency decompo sed signals as intra-hour, intra-day, and slow-cycling components, respectively, as expressed in the following:

$$p_{\mathrm{hf},t} = \sum_{j=1}^{3} D_{j,t} \tag{10}$$

$$p_{\mathrm{mf},t} = \sum_{j=4}^{8} D_{j,t} \tag{11}$$

$$p_{\mathrm{lf},t} = A_{8,t}. \tag{12}$$

$p_{\mathrm{hf},t}$ is the high frequency or intra-hour component as shown in (10). As shown, it is the summation of first to third detailed signals. It changes every 5 min and its period is 40 min, which is less than an hour. This signal is appropriate to control large-scale batteries, such as NaS, that has high ramp rates and less energy capacity compared to CAES. $p_{\mathrm{mf},t}$ is the medium frequency or intra-day component as defined in (11). This signal changes every 40 min and its period is 21 h and 20 min, which is less than a day. Hence, it is a good candidate for intra-day component to charge and discharge mechanical large-scale energy storage units as CAES. $p_{\mathrm{lf},t}$ is the low frequency or slow-cycling component that changes every 21 h and 20 min as shown in (11). This can be easily followed by conventional generators.

B. Energy Storage Sizing Algorithm Based on DFT

Step 1) Find $p_{\mathrm{wfe},t}$ as described in (8).
Step 2) Find the DFT of $p_{\mathrm{wfe},t}$ to project the signal from time domain to frequency domain using (1).
Step 3) Use the high pass, band pass, and low pass filters, as described in Table I, to extract high-, medium-, and low-frequency components. Cut-off frequencies were chosen to match the DWT method. Hence, the results of the two methodologies can be compared and the tradeoff can be discussed.
Step 4) Take the inverse DFT of the decomposed components in the previous step and change them from frequency domain to time domain using (2).

C. Applying Large-Scale Energy Storage Properties

Each energy storage technology has its own operating limits. These characteristics are shown in Table II for NaS and CAES.

TABLE II
ENERGY STORAGE TECHNOLOGIES CHARACTERISTICS [26], [27]

Energy storage technology	NaS	CAES
Power capacity (MW)	50	300
Energy capacity (MWh)	300	6000
Max ramp up/down rate (MW/min)	50	18
Efficiency (%)	75	70
Required idle time to switch mode (min)	–	20
Max state of charge (%)	0.9	1
Min state of charge (%)	0.1	0

In particular, CAES needs at least 20 min to remain idle for switching between modes [26].

In the literature [19], [20], and [22], the sizing based on signal processing approach neglects all energy storage characteristics. Hence, the rated power and energy capacity are sized to follow the components completely as follows:

$$P = \max\left(|c_t|\right) \tag{13}$$

$$\mathrm{SoC}_t = \sum_{i=1}^{t} c_i \quad \forall t \tag{14}$$

$$E = \max(\mathrm{SoC}_t) - \min(\mathrm{SoC}_t) \tag{15}$$

where

c_t decomposed component at time t in MW;
P rated power capacity in MW;
SoC_t state of charge at time t in MW;
E rated energy capacity in MWh.

This paper considers energy storage characteristics that prevent energy storage to closely follow the control signal. The intra-day component controls CAES operation. NaS battery follows the intra-hour component and also the difference between CAES output and the intra-day component. The detailed steps of the algorithm are described as follows.

Step 1) Consider medium frequency (intra-day) signal to control CAES operation

$$p_t = p_{\mathrm{mf},t} \quad \forall t \tag{16}$$

where $p_t$is the energy storage operation at time t in MW.

Step 2) Set $t = 1$ to start scheduling. This paper has considered the initial state of the charge before running the simulation to be 50% of the full energy capacity.

Step 3) Operational power limit: The charge and discharge power of energy storage is limited to its rated power capacity

$$\text{if } |p_t| > P_r N, \quad \text{then } p_t = \mathrm{sign}(p_t) P_r N \tag{17}$$

where

P_r rated energy storage power capacity;
N number of energy storage units.

Step 4) Ramp rate limit: When $t > 1$

$$r_t = (p_t - p_{t-1})/\Delta t \tag{18}$$

$$\text{if } |r_t| > R_r N, \quad \text{then } p_t = p_t + \mathrm{sign}(r_t) R_r N \tag{19}$$

where

r_t energy storage ramp rate at time t in MW/min;
R_r rated ramp rate in MW/min.

Step 5) Remain idle for switching between charging and discharging modes (this is only applicable to CAES)

$$\text{if } p_t p_{t-1} < 0, \text{ then } p_k = 0,\ k \in [t, t + \text{idletime}]. \tag{20}$$

Step 6) State of the charge limit

$$\mathrm{SoC}_t = \begin{cases} (p_t \eta \Delta t)/E_r + \mathrm{SoC}_{t-1}, & \text{if } p_t > 0 \\ (p_t \Delta t)/E_r + \mathrm{SoC}_{t-1}, & \text{if } p_t < 0 \end{cases} \tag{21}$$

$$\text{if } \mathrm{SoC}_t > \mathrm{SoC}_{\max}, \text{ then } \mathrm{SoC}_t = \mathrm{SoC}_{\max},\ p_t = E_r(\mathrm{SoC}_t - \mathrm{SoC}_{t-1})/(\eta \Delta t) \tag{22}$$

$$\text{if } \mathrm{SoC}_t < \mathrm{SoC}_{\min}, \text{ then } \mathrm{SoC}_t = \mathrm{SoC}_{\min},\ p_t = E_r(\mathrm{SoC}_t - \mathrm{SoC}_{t-1})/\Delta t \tag{23}$$

where

$\mathrm{SoC}_{\min}$ minimum state of charge in %;
$\mathrm{SoC}_{\max}$ maximum state of charge in %;
E_r rated energy capacity in MWh;
η efficiency in %.

Step 7) Check if the simulation has reached the end: If $t < T$, then, $t = t + 1$, go to Step 3), else, $p_{C,t} = p_t \quad \forall t$ and go to Step 8) where

T whole period of simulation;
$p_{C,t}$ CAES operation at time t in MW.

Step 8) NaS battery is supposed to provide the high-frequency (intra-hour) component and the difference between CAES operation and medium-frequency component as follows:

$$p_t = p_{\mathrm{hf},t} + (p_{\mathrm{mf},t} - p_{C,t}) \quad \forall t \tag{24}$$

where p_t is the NaS control signal at time t in MW.

Step 9–12) Be the same as Steps 2)–6) except for Step 5).

Step 13) Check if the simulation has reached the end: If $t < T$, then, $t = t + 1$, go to Step 9), else, $p_{N,t} = p_t \quad \forall t$ and go to Step 14). where $p_{N,t}$ is the NaS operation at time t in MW.

Step 14) Calculating wind spill and back-up energy: The residual forecast error signal is defined in (25). It is the difference between summation of high- and medium-frequency components with the summation of NaS and CAES operation. The wind spill and back-up energy are defined as positive and negative parts of this signal, respectively, shown in (26) and (27):

$$p_{r,t} = p_{\mathrm{hf},t} + p_{\mathrm{mf},t} - (p_{N,t} + p_{C,t}) \tag{25}$$

$$p_{\mathrm{ws},t} = \left(|p_{r,t}| + p_{r,t}\right)/2 \tag{26}$$

$$p_{\mathrm{rs},t} = \left(|p_{r,t}| - p_{r,t}\right)/2 \tag{27}$$

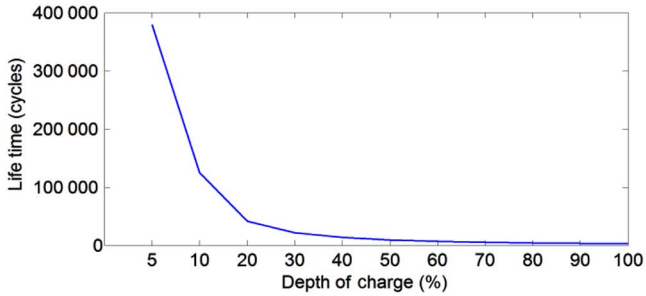

Fig. 1. NaS battery number of cycles to failure with respect to DoD [31].

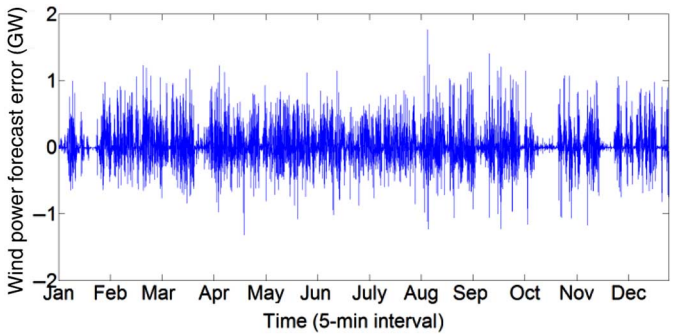

Fig. 2. BPA wind power forecast error of BPA for the whole year of 2013.

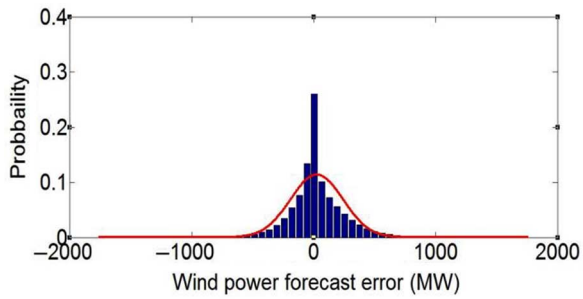

Fig. 3. BPA wind power forecast error histogram for 2013.

TABLE III
WIND POWER FORECAST ERROR SIGNAL CHARACTERISTICS

Max (MW)	Min (MW)	Max ramp up/down (MW/5min)	Mean (MW)	Sigma (MW)
1763	−1316	805/−875	28	216

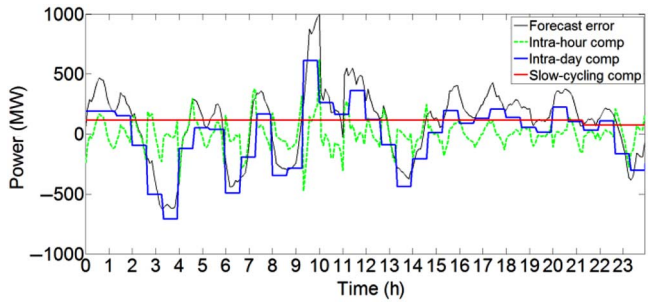

Fig. 4. Forecast error and DWT components for a day in January 2013.

where

$p_{r,t}$	residual power at time t in MW;
$p_{\mathrm{ws},t}$	wind spill power at time t in MW;
$p_{\mathrm{rs},t}$	back-up power at time t in MW.

IV. Battery Life Cycle Analysis

When batteries are used to mitigate renewable generation challenges, they cycle frequently to keep up with renewable ramp rates and mitigate the forecast error. Battery service life depends on cycles at each depth of discharge (DoD). Cycle counting has different methods as described in ASTM E 1049-85 [28]. This paper uses rain-flow cycle counting, which was first proposed by Downing and Socie [29] and mentioned in ASTM E 1049-85. The number of cycles at each depth of discharge including complete and partial cycles is the result of this algorithm.

To study the impact of cycles on battery service life, first DoD is divided to m interval. Then, the number of cycles in a year for each range of DoD is extracted from NaS operation derived from algorithms in Section III by implementing rain-flow cycle counting method. Finally, the battery lifetime in years is calculated from number of cycles and number of cycles to failure at each DoD as follows [30]:

$$\mathrm{Life}_{\mathrm{NaS}} = 1/\sum_{i=1}^{m} {}^{N_i}/_{\mathrm{CF}_i} \tag{28}$$

where

$\mathrm{Life}_{\mathrm{NaS}}$	NaS battery lifetime in years;
N_i	number of cycles at each DoD;
CF_i	number of cycles to failure at each DoD;
m	number of DoD ranges.

The number of cycles to failure at each DoD for NaS battery is depicted in Fig. 1. As shown, cycles with higher DoD have more impacts on battery lifetime depreciation than cycles with lower DoD.

V. Case Study and Discussion

The forecast error is determined by the actual and hour-ahead wind forecast data with 5-min interval of the BPA area in 2013 [32]. Since wind power forecast errors are not repetitive over multiple years, such analyses need to be repeated over many years to get a broader understanding of wind power output characteristics for a particular service area. The BPA-installed wind capacity was 4.5 GW in 2013. The wind power forecast error signal is shown in Fig. 2 for the whole year of 2013. The normalized histogram of this signal and the normal distribution function that fits are depicted in Fig. 3. The wind power forecast error signal characteristics are summarized in Table III.

The intra-hour, intra-day, and slow-cycling components of wind power forecast error signal are extracted and shown in Figs. 4 and 5 by DWT and DFT, respectively. As shown, the time resolution of the signal processing technique is 5-min—the same as time resolution of the wind power forecast data. This time resolution seems good enough for subhourly dispatch

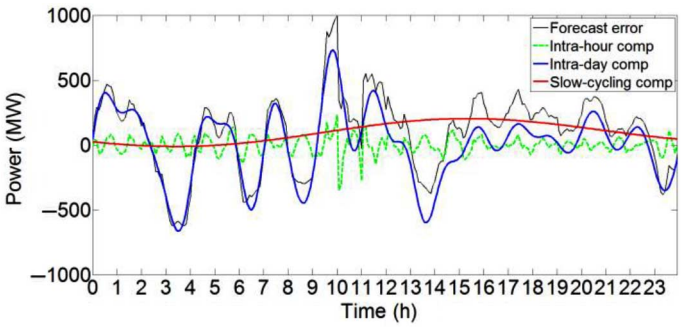

Fig. 5. Forecast error and its DFT components for a day in January 2013.

TABLE IV
DWT AND DFT COMPONENTS CHARACTERISTICS

Method	Component	Max (MW)	MIN (MW)	Max ramp up/down (MW/5 min)	Mean (MW)	Sigma (MW)
DWT	Intra-hour	912	−779	966/−936	0	67
	Intra-day	964	−1065	987/−1394	0	191
	Slow-cycling	275	−153	296/−312	28	74
DFT	Intra-hour	978	−572	778/−749	0	46
	Intra-day	972	−1048	207/−160	0	182
	Slow-cycling	382	−303	6/−6	28	106

TABLE V
DWT AND DFT SIZING RESULTS BASED ON THE LITERATURE APPROACH

Method	Component	Power (MW)	ENERGY (MWH)
DWT	Intra-hour	912	279
	Intra-day	1,065	4,776
DFT	Intra-hour	978	187
	Intra-day	1,048	2,265

(5-min dispatch) of grid-scale energy storage technologies as NaS and CAES. The difference between DFT and DWT methodologies is the shape of decomposed components. The properties of decomposed components are shown in Table IV. As shown, the mean values of the intra-hour and intra-day components are zero, which is desirable to control energy storage. The mean of slow-cycling components are equal to the wind forecast error mean shown in Table III.

According to three sigma rule, 99% of the time the value of the intra-day component is between ± 573 MW for DWT method and ± 546 MW for DFT method. The statistical sizing approach based on three sigma rule results in four 50-MW NaS and two 300-MW CAES (based on the numbers presented in Table IV). Also, 99% of the time the value of intra-hour component is between ± 201 MW for the DWT method and ± 138 MW for the DFT method. Hence, based on this statistical evaluation, four and three 50-MW NaS are required for DWT and DFT methods, respectively. This statistical evaluation neglects all the operational energy storage limits except for rated power capacity, and only based on standard deviation of components.

The required energy storage based on [19], [20], and [22] is shown in Table V. According to the results shown in Table V, twenty 50-MW NaS and 300-MW CAES are required to follow the intra-hour and intra-day components, respectively. This approach results in oversizing energy storage units compared

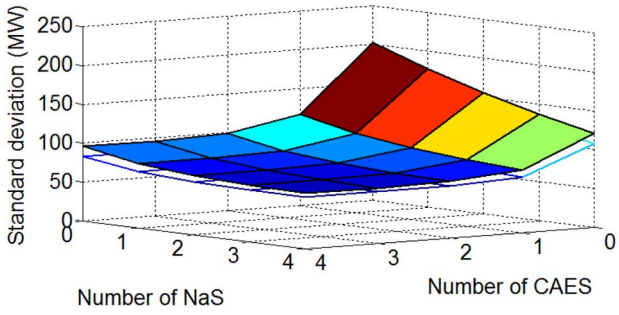

Fig. 6. Standard deviation of the residual forecast error by DWT and DFT.

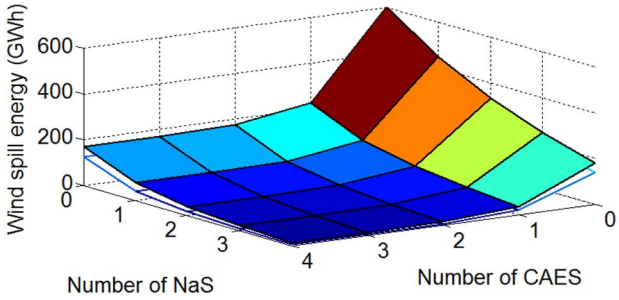

Fig. 7. Wind spill energy by DWT and DFT methods.

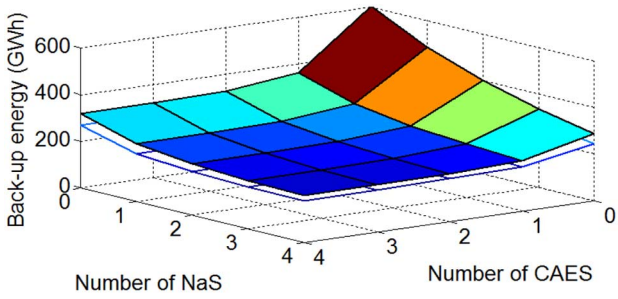

Fig. 8. Back-up energy by DWT and DFT methods.

to statistical approach, because of neglecting statistical characteristics of components and fully following even the infrequent values. The resultant size of energy storage units cannot even fully compensate control signals due to neglecting all energy storage operational barriers.

This paper approaches energy storage sizing by studying the impacts of different combinations of NaS and CAES on reducing wind spill and required back-up energy. Algorithms defined in Section III are used to simulate 25 different scenarios by varying number of 300 MW CAES and 50 MW NaS units from zero to four. The standard deviation, wind spillage, and required back-up energy are depicted in Figs. 6–8. As one can observe, the slopes in these figures decrease by increasing the size of energy storage units and becomes horizontal at the end. This observation proves the sufficient number of scenarios. DFT and DWT results are shown in white and colored surfaces, respectively. Since DFT components are not restricted to be constant for a specific duration compared to DWT by Haar wavelet function, DFT results have better performance than DWT results.

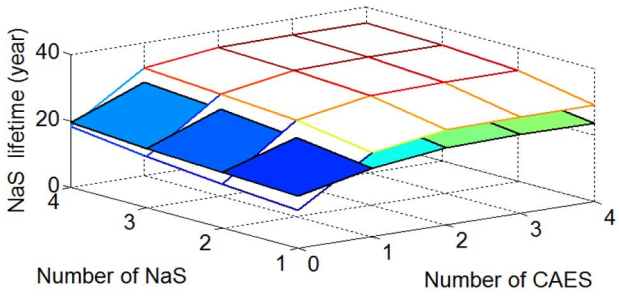

Fig. 9. NaS lifetime in years by DFT and DWT methods.

Standard deviation decreases from 202 to 70 MW for DWT by implementing four NaS and CAES units as shown in Fig. 6. It also decreases from 187 to 66 MW for DFT by implementing four NaS and CAES units. As shown, the standard deviation decrease becomes less by increasing energy storage units and the surface becomes flat eventually.

Wind spill energy reduces from 600 to 11 GWh for DWT method by increasing the number of energy storage units, as shown in Fig. 7. It also reduces from 600 to 4 GWh for DFT method by increasing the number of energy storage units. The required back-up energy decreases from 600 to 198 GWh for DWT method and reduces to 178 GWh for DFT approach, as shown in Fig. 8. The reason why back-up energy reduction is less than wind spill energy reduction is because of considering energy storage efficiency. Hence, the storage is able to charge the excess wind energy, but it cannot discharge as required. The slope of surfaces decreases and becomes flat by increasing the number of energy storage units.

The impact of energy storage size on the NaS battery lifetime is analyzed and shown in Fig. 9. The cycle counting and battery lifetime estimation is very important for planning large-scale batteries. According to the results, by increasing the number of NaS battery units, their lifetime increases. This is due to increasing the energy capacity of the total batteries. Hence, there is less number of cycles at each range of DoD. This number increases from 16 to 20 years for DWT, and 12 to 18 years for the DFT method by increasing the number of NaS battery units from one to four while considering no CAES units. When implementing CAES, NaS battery lifetime increases. It increases from 16 to 23 years when the number of CAES units increases from zero to four, while having one NaS for DWT method. This number changes from 12 to 30 years for DFT method. Hence, the NaS battery lifetime increases by CAES contribution, which can follow intra-day component. NaS battery lifetime increases from 16 to 30 years for DWT and 12 to 35 years for DFT, while increasing the CAES units from zero to four and NaS units from one to four. This result is very beneficial for calculating the net present value of battery investment for a long-time project by knowing the number of battery replacements during the whole project.

The impact of considering 100 MW frequency bias constant on reducing the wind power forecast error impacts are shown in Figs. 10–12. This 100 MW allowable mismatch is considered for the residual of wind power forecast error after implementing energy storage units. As shown in Fig. 10, the standard deviation of wind power forecast error without implementing

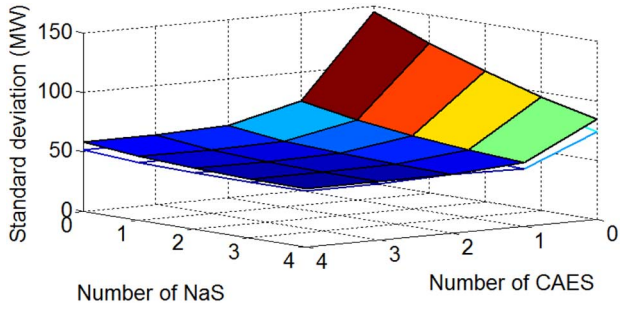

Fig. 10. Standard deviation of the residual forecast error considering frequency bias constant for DWT/DFT.

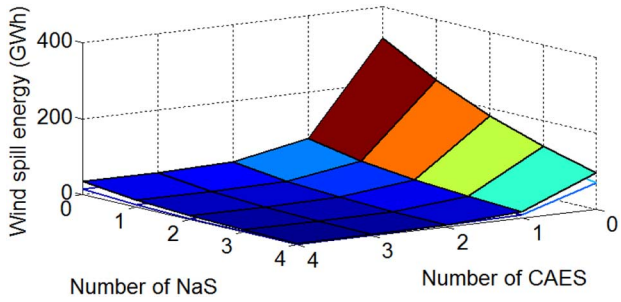

Fig. 11. Wind spill energy considering frequency bias constant for DWT/DFT.

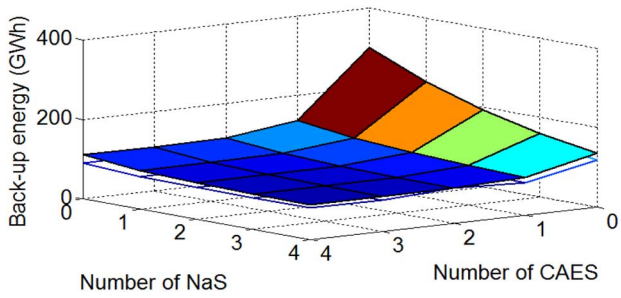

Fig. 12. Back-up energy considering frequency bias constant for DWT/DFT.

energy storage is 145 MW for DWT and 131 MW for DFT, which was about 200 MW before considering frequency bias constant. It will reduce to 48 MW for DWT and 46 MW for DFT by implementing four CAES and NaS units. As shown in Fig. 11, wind spill energy without energy storage is 320 GWh for DWT and 275 GWh for DFT method. As shown in Fig. 12, the required back-up energy considering frequency bias constant is 300 GWh for DWT and 267 GWh for DFT. Hence, by considering the frequency bias constant, wind spill and required back-up energy decreases about 300 GWh for the no-storage case.

VI. Conclusion

This paper proposes and compares two signal processing methods (based on DFT and DWT) to schedule hybrid configuration of energy storage technologies (e.g., NaS battery and CAES) and conventional generators. The defined DWT method results in step-shape components, which are more appropriate for controlling large-scale mechanical energy storage units that cannot change their output frequently. Hence, scheduling

based on DWT results in more wind spillage and requires more back-up energy compared to DFT method that varies every interval.

The proposed approach is based on analyzing the impacts of increasing the number of energy storage units on reducing wind spillage and the required back-up energy. Also, the standard deviation of the residual wind power forecast signal is studied, which is an important factor for planning the extra required system flexibility. This approach avoids oversizing the required energy storage by implementing different combinations of energy storage units and analyzing their impacts. Frequency bias constant is considered to reduce the final wind spill and needed back-up energy.

The detailed properties of CAES and NaS units, including efficiency, rated power and energy capacity, DoD (only applied to NaS), and required idle time for switching between charging and discharging modes (only applied to CAES) are considered. NaS battery service life depends on the cycles at each DoD. The NaS battery lifetime increases by adding more NaS and CAES units.

The information provided in this paper is beneficial for investors in energy storage and wind sectors. The overall energy storage sizing depends on the economic issues of energy storage operation, investment costs, and wind production tax credit in addition to analyzing the technical issues.

REFERENCES

[1] F. Lauha, S. Steve, S. Sgruti, and Q. Limig, "Global Wind Report–Annual Market Update 2013," Global Wind Energy Council, Brussels, Belgium, 2012.

[2] P. Meibom, K. B. Hilger, H. Madsen, and D. Vinther, "Energy comes together in Denmark: The key to a future fossil-free Danish power system," *IEEE Power Energy Mag.*, vol. 11, no. 5, pp. 46–55, Sep./Oct. 2013.

[3] H. T. Le, S. Santoso, and T. Q. Nguyen, "Augmenting wind power penetration and grid voltage stability limits using ESS: Application design, sizing, and a case study," *IEEE Trans. Power Syst.*, vol. 27, no. 1, pp. 161–171, Feb. 2012.

[4] C. Abbey and G. Joos, "A stochastic optimization approach to rating of energy storage systems in wind-diesel isolated grids," *IEEE Trans. Power Syst.*, vol. 24, no. 1, pp. 418–426, Apr. 2009.

[5] Y. Levron, J. M. Guerrero, and Y. Beck, "Optimal power flow in micro grids with energy storage," *IEEE Trans. Power Syst.*, vol. 28, no. 3, pp. 3226–3234, Apr. 2013.

[6] D. Gayme and U. Topcu, "Optimal power flow with large-scale storage integration," *IEEE Trans. Power Syst.*, vol. 28, no. 2, pp. 709–717, May 2013.

[7] S. Teleke, M. E. Baran, S. Bhattacharya, and A. Q. Huang, "Rule-based control of battery energy storage for dispatching intermittent renewable sources," *IEEE Trans. Sustain. Energy*, vol. 1, no. 3, pp. 117–124, Oct. 2010.

[8] L. Xu, X. Ruan, C. Mao, B. Zhang, and Y. Luo, "An improved optimal sizing method for wind-solar-battery hybrid power system," *IEEE Trans. Sustain. Energy*, vol. 4, no. 3, pp. 774–785, Jul. 2013.

[9] T. K. A. Brekken, A. Yokochi, A. V. Jouanne, Z. Z. Yen, H. M. Hapke, and D. A. Halamay, "Optimal energy storage sizing and control for wind power applications," *IEEE Trans. Sustain. Energy*, vol. 2, no. 1, pp. 69–77, Jan. 2011.

[10] S. Teleke, M. E. Baran, A. Q. Huang, S. Bhattacharya, and L. Anderson, "Control strategies for battery energy storage for wind farm dispatching," *IEEE Trans. Energy Convers.*, vol. 24, no. 3, pp. 725–732, Sep. 2009.

[11] P. Wang, Z. Gao, and L. Bertling, "Operational adequacy studies of power systems with wind farms and energy storages," *IEEE Trans. Power Syst.*, vol. 27, no. 4, pp. 2377–2384, Nov. 2012.

[12] C. Wang, Z. Lu, and Y. Qiao, "A consideration of the wind power benefits in day-ahead scheduling of wind-coal intensive power systems," *IEEE Trans. Power Syst.*, vol. 28, no. 1, pp. 236–245, Feb. 2013.

[13] M. Ghofrani, A. Arabali, M. Etezadi-Amoli, and M. S. Fadali, "Energy storage application for performance enhancement of wind integration," *IEEE Trans. Power Syst.*, vol. 28, no. 4, pp. 4803–4811, Nov. 2013.

[14] S. Teleke, M. E. Baran, S. Bhattacharya, and A. Q. Huang, "Rule-based control of battery energy storage for dispatching intermittent renewable sources," *IEEE Trans. Sustain. Energy*, vol. 1, no. 3, pp. 117–124, Oct. 2010.

[15] S. Mei, Y. Wang, F. Liu, X. Zhang, and Z. Sun, "Game approaches for hybrid power system planning," *IEEE Trans. Sustain. Energy*, vol. 3, no. 3, pp. 506–517, Jul. 2012.

[16] S. Mei, D. Zhang, Y. Wang, F. Liu, and W. Wei, "Robust optimization of static reserve planning with large-scale integration of wind power: A game theoretic approach," *IEEE Trans. Sustain. Energy*, vol. 5, no. 2, pp. 535–545, Apr. 2014.

[17] X. Ke, N. Lu, and C. Jin, "Control and size energy storage systems for managing energy imbalance of variable generation resources," *IEEE Trans. Sustain. Energy*, vol. 6, no. 1, pp. 70–78, Jan. 2015.

[18] F. Luo, K. Meng, Z. Y. Dong, Y. Zheng, Y. Chen, and K. P. Wong, "Coordinated operational planning for wind farm with battery energy storage system," *IEEE Trans. Sustain. Energy*, vol. 6, no. 1, pp. 253–262, Jan. 2015.

[19] Y. V. Makarov, P. Du, M. C. W. Kintner-Meyer, J. Chunlian, and H. F. Illian, "Sizing energy storage to accommodate high penetration of variable energy resources," *IEEE Trans. Sustain. Energy*, vol. 3, no. 1, pp. 34–40, Jan. 2012.

[20] J. Xiao, L. Bai, F. Li, H. Liang, and C. Wang, "Sizing of energy storage and diesel generators in an isolated microgrid using discrete Fourier transform (DFT)," *IEEE Trans. Sustain. Energy*, vol. 5, no. 3, pp. 907–916, Jul. 2014.

[21] P. Mandal, A. U. Haque, J. Meng, A. K. Srivastava, and R. Martinez, "A novel hybrid approach using wavelet, firefly algorithm, and fuzzy ARTMAP for day-ahead electricity price forecasting," *IEEE Trans. Power Syst.*, vol. 28, no. 2, pp. 1041–1051, May 2013.

[22] Q. Jiang and H. Hong, "Wavelet-based capacity configuration and coordinated control of hybrid energy storage system for smoothing out wind power fluctuations," *IEEE Trans. Power Syst.*, vol. 28, no. 2, pp. 1363–1372, May 2013.

[23] S. R. Mohanty, N. Kishor, P. K. Ray, and J. P. S. Catalao, "Comparative study of advanced signal processing techniques for islanding detection in a hybrid distributed generation system," *IEEE Trans. Sustain. Energy*, vol. 6, no. 1, pp. 122–131, Jan. 2015.

[24] R. X. Gao and R. Yan, *Wavelets: Theory and Applications for Manufacturing*. New York, NY, USA: Springer, 2010.

[25] C. Loutan, California ISO, private communication, Apr. 11, 2014.

[26] F. S. Barnes and J. G. Levine, *Large Scale Energy Storage Handbook*. Boca Raton, FL, USA: CRC Press, Mar. 2011.

[27] R. Carnegie, D. Gotham, D. Nderitu, and P. V. Preckel. (2013, Jun.). *Utility Scale Energy Storage Systems, Benefits, Application, and Technologies*, State Utility Forecasting Group, West Lafayette, Indiana [Online]. Available: http://www.purdue.edu/discoverypark/energy/assets/pdfs/SUFG/publications/SUFG%20Energy%20Storage%20Report.pdf

[28] ASTM E 1049-85. (Reapproved 2011), *Standard Practices for Cycle Counting in Fatigue Analysis*. American society for testing and materials (ASTM) International, West Conshohocken, PA, USA, 2011.

[29] S. D. Downing and D. F. Socie, "Simple rain flow counting algorithms," *Int. J. Fatigue*, vol. 4, pp. 31–40, 1982.

[30] R. Dufo-López, J. L. Bernal-Agustín, and J. A. Domínguez-Navarro, "Generation management using batteries in wind farms: Economical and technical analysis for Spain," *IET Energy Policy*, vol. 37, no. 1, pp. 126–139, Aug. 2009.

[31] N. Lu, M. R. Weimar, Y. V. Makarov, J. Ma, and V. V. Viswanathan, "The wide-area energy storage and management system—Battery storage evaluation," PNNL-18679, Pacific Northwest National Laboratory, Richland, WA, USA, 2009.

[32] *Historical Data of Total Wind Generation and Wind Forecast in 2013*, Bonneville Power Administration (BPA) Balancing Authority, Portland, OR, USA [Online]. Available: http://transmission.bpa.gov/business/operations/wind/

Hamideh Bitaraf (S'11) received the B.S. and M.S. degrees in electrical engineering from Sharif University of Technology, Tehran, Iran, in 2010 and 2012, respectively. She is currently pursuing the Ph.D. degree at the Bradley Department of Electrical and Computer Engineering, Virginia Polytechnic and State University, Blacksburg, VA, USA.

Since 2012, she has been a Graduate Research Assistant with the Advanced Research Institute, Arlington, VA, USA. Her research interests include energy storage, wind power, demand response, renewable energy, smart grid, and optimization methods.

Saifur Rahman (S'75–M'78–SM'83–F'98) received the B.Sc. degree in electrical engineering from the Bangladesh University of Engineering & Technology, Dhaka, Bangladesh, in 1973, the M.S. degree in electrical engineering from the State University of New York, Stony Brook, NY, USA, in 1975, and the Ph.D. degree in electrical engineering from the Virginia Polytechnic Institute and State University (Virginia Tech), Blacksburg, VA, USA, in 1978.

He is the Founding Director of the Advanced Research Institute, Virginia Tech, Arlington, VA, USA, where he is the Joseph R. Loring Professor of Electrical and Computer Engineering. He is also the Director of the Center for Energy and the Global Environment.

Prof. Rahman is the Founding Editor-in-Chief of the IEEE ELECTRIFICATION MAGAZINE. He was also the Founding Editor-in-Chief of the IEEE TRANSACTIONS ON SUSTAINABLE ENERGY. He served as a Vice President of the IEEE Power and Energy Society (PES) from 2009 to 2013 and is currently serving as a member of the Board of Governors of the IEEE Society on Social Implications of Technology. In 2006, he served on the IEEE Board of Directors as the Vice President for Publications. He served as the Chair of the U.S. National Science Foundation Advisory Committee for International Science and Engineering from 2010 to 2013. He is a Distinguished Lecturer for the IEEE PES, and has lectured on smart grid, energy efficiency, renewable energy, demand response, distributed generation, and critical infrastructure protection topics in over 30 countries on all six continents. He was the recipient of the IEEE Millennium Medal.

Manisa Pipattanasomporn (S'01–M'06–SM'11) received the B.S. degree in electrical engineering from Chulalongkorn University, Bangkok, Thailand, in 1999, the M.S. degree in energy economics and planning from the Asian Institute of Technology (AIT), Bangkok, Thailand, in 2001, and the Ph.D. degree in electrical engineering from Virginia Polytechnic Institute and State University (Virginia Tech), Blacksburg, VA, USA, in 2004.

She joined the Department of Electrical and Computer Engineering, Virginia Tech, as an Assistant Professor in 2006. She serves as one of the Principal Investigators (PIs) of multiple research Grants from the U.S. National Science Foundation, the U.S. Department of Defense, and the U.S. Department of Energy, on research topics related to smart grid, microgrid, energy efficiency, load control, renewable energy, and electric vehicles. Her research interests include renewable energy systems, energy efficiency, distributed energy resources, and smart grid.